Depth-resolved confocal micro-Raman spectroscopy for characterizing GaN-based light emitting diode structures

Wei-Liang Chen, Yu-Yang Lee, Chiao-Yun Chang, Huei-Min Huang, Tien-Chang Lu, and Yu-Ming Chang

---

Depth-resolved confocal micro-Raman spectroscopy for characterizing GaN-based light emitting diode structures

Wei-Liang Chen,[1] Yu-Yang Lee,[1] Chiao-Yun Chang,[2] Huei-Min Huang,[2] Tien-Chang Lu,[2] and Yu-Ming Chang[1,a)]

[1]*Center for Condensed Matter Sciences, National Taiwan University, 10617 Taipei, Taiwan*
[2]*Department of Photonics, National Chiao Tung University, 30010 Hsinchu, Taiwan*

In this work, we demonstrate that depth-resolved confocal micro-Raman spectroscopy can be used to characterize the active layer of GaN-based LEDs. By taking the depth compression effect due to refraction index mismatch into account, the axial profiles of Raman peak intensities from the GaN capping layer toward the sapphire substrate can correctly match the LED structural dimension and allow the identification of unique Raman feature originated from the 0.3 μm thick active layer of the studied LED. The strain variation in different sample depths can also be quantified by measuring the Raman shift of GaN A_1(LO) and E_2(high) phonon peaks. The capability of identifying the phonon structure of buried LED active layer and depth-resolving the strain distribution of LED structure makes this technique a potential optical and remote tool for *in operando* investigation of the electronic and structural properties of nitride-based LEDs. © *2013 AIP Publishing LLC.* [http://dx.doi.org/10.1063/1.4829627]

I. INTRODUCTION

In the development of light emitting diodes, III-nitride based heterostructures, such as $In_x Ga_{1-x}N$/GaN supperlattices (SLs) and multi-quantum wells (MQWs), have been successfully and widely used as the active layer of GaN-based LED.[1] This III-nitride based active layer greatly increases the light emission efficiency and allows a wide tuning range of the light emitting wavelength from UV to NIR. However, one important aspect for improving the light emission strength of GaN-based LEDs is to reduce the local defect density and strain in these SLs and MQWs to eliminate the electric polarization fields.[1,2] Another challenge is to understand the droop mechanism in the active layer which results in the reduction of light emission efficiency when LED is operated under high current density.[3] Conventional material characterization techniques such as scanning electron microscopy (SEM) and transmission electron microscopy (TEM) always require sample preparation in order to explore the buried active layer of LEDs. Recently, there is an increasing demand to measure directly the active layer of actual LED structures to realize the electronic and structural properties, which strongly influence device performances.[4,5]

In this work, we propose to construct a depth-resolved confocal micro-Raman microscope,[6,7] which follows the principle of confocal optics and is capable of performing the optical sectioning function with ultimate depth resolution. In tradition, depth-resolved confocal optical microscope has widely been used in biological studies, but its applications in condensed matter sciences and actual optoelectronic devices are still quite rare.[6–8] On the other hand, Raman spectroscopy has been demonstrated to be a powerful optical technique for the investigation of lattice structural and electronic

properties of condensed matters, because it requires minimal sample preparation and is not invasive.[9] The combination of Raman spectroscopy with a depth-resolved confocal microscope will create a novel tool for scientists, particularly material scientists and engineers, to explore the physical properties, such as local defects, strain distributions, and crystalline qualities, of embedded semiconductor heterostructures.[8,10–12]

To demonstrate the aforementioned capabilities, we use a designed GaN-based LED structure as reference sample and successfully reveal the depth-dependent phonon structure of its active layer. In this work, we find out that the effect of refraction index mismatch between the investigated sample and the objective immersion medium needs to be taken into account to correctly interpret the axial focal position and axial resolution.[13] The depth compression effect due to the refraction index mismatch is particular significant for high refraction index materials such as III-nitride and IV-group semiconductors. We remark that the depth-resolved confocal micro-Raman spectroscopy after correctly accounting for the depth compression effect can produce depth-dependent Raman peak intensity profiles, consistent with the corresponding LED layer structure. Furthermore, the depth-dependent Raman spectrum exhibits a unique Raman spectral feature, which can be clearly assigned to the sub-micron thin active layer of the LED sample. The detail analysis of the spectral line frequency shift of GaN A_1(LO) and E_2(high) phonon peaks reveals the GaN strain distribution as a function of the sample depth.

II. EXPERIMENTAL METHODS

A. Sample description

In this study, an actual GaN-based LED structure was designed and grown on the c-plane sapphire substrate by using metal organic chemical vapor deposition system

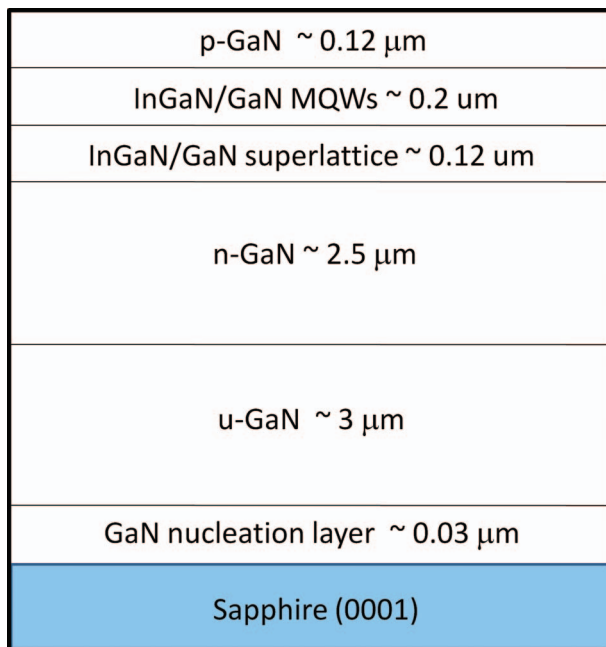a)Author to whom correspondence should be addressed. Electronic mail: ymchang@ntu.edu.tw

FIG. 1. Layer structure of the studied GaN-based LED sample. The total thickness of the MOCVD grown layers is ∼6 μm.
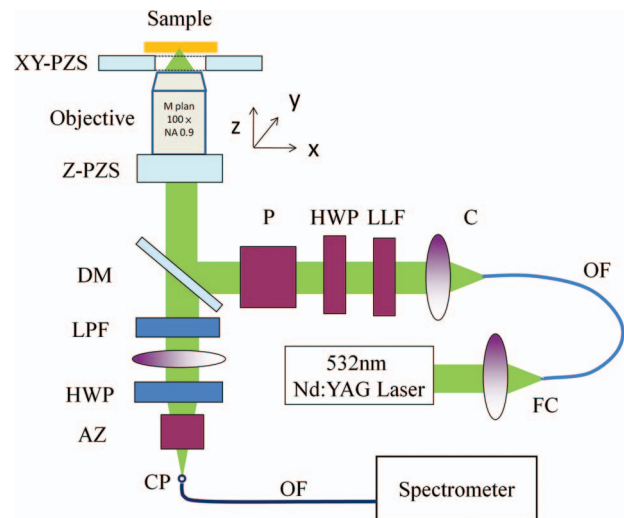

FIG. 2. Experimental configuration for performing depth-resolved confocal micro-Raman spectroscopy, where the notations denote: FC-fiber coupler, OF-optical fiber, C-collimator, LLF-laser line filter, HWP-half-wave plate, P-polarizer, DM-dichroic mirror, PZS-piezo stage, LPF-long pass filter, AZ-analyzer, and CP-confocal pinhole.

(MOCVD). Figure 1 illustrates the sample layer structure in detail, where the layer structure includes a 30 nm GaN nucleation layer, 3 μm of undoped GaN, and 2.5 μm of Si-doped n-GaN from the substrate toward the surface. For the LED active layer, 20 pairs of $In_{0.05}Ga_{0.95}N$/GaN superlattice structure are inserted prior to the growth of the InGaN/GaN multi-quantum wells (MQWs). The MQWs are separated into two groups: the first group consists of 6 wells with an 8% In content, while the second group consists of subsequent 9 pairs with a 15% In content. The InGaN well sizes are 2.5–3 nm and the GaN barriers are 12 nm thick for both groups. Note that the former InGaN MQWs facilitate uniform distribution of carriers across the active layers, while the latter InGaN MQWs dominate the carrier radiative recombination. This active layer structure can significantly improve the LED's light emission efficiency.[14–16] Finally, 0.12 μm of Mg doped p-GaN serve as the capping layer.

B. Depth-resolved confocal micro-Raman microscope system

Figure 2 shows a schematic diagram of our home-built depth-resolved confocal micro-Raman microscope system. The excitation light source is a diode-pumped 532 nm, continuous wave, and 100 mW Nd:YAG laser. The choice of this laser wavelength is to ensure the LED sample is transparent under the laser irradiation and preserve the validity of the confocal principle. The laser output is coupled into an optical fiber and collimated with a fiber coupler to expand the beam size up to ∼10 mm. The laser beam passes through a laser line filter and a pair of 532 nm half-waveplate and polarizer for power and polarization control before it is sent into the back-port of the optical microscope (Nikon TE2000U). In the microscope carousel, a long pass dichroic

beamsplitter reflects the laser beam onto the back aperture of the objective (Olympus MPlan, 100×, NA0.9) which focuses the light onto the sample. Note that it is necessary for the laser beam to overfill the back aperture of the objective to make full use of the objective numerical aperture (NA) and achieve the optimal lateral and axial resolutions of the objective. The Raman signal is collected by the same objective, then passed through a long pass filter, and focused into the aperture of an optical fiber (50 μm core diameter) via the microscope tube lens ($f = 20$ cm). In this configuration, the aperture of the optical fiber serves as the confocal pinhole whose size governs the depth discrimination of the system. The optical fiber is then connected to the spectrometer system (Jobin-Yvan FHR640 + LN$_2$ cooled Symphony CCD) for Raman measurement. To perform depth-resolved Raman measurement, the objective is mounted on a single-axis piezo stage to vary the laser focusing depth. A customer-designed LabVIEW program controls the piezo stage movement in coordination with the Raman spectrum acquisition.

III. EXPERIMENTAL RESULTS AND DISCUSSIONS

A. Depth resolution of confocal micro-Raman microscope system

The depth resolution of our confocal micro-Raman microscope system is characterized by scanning the objective in the z-axial direction and measuring the laser reflection from a silicon sample. Figure 3 shows that the axial profile of the reflected laser signal as a function of the axial position of the objective. The axial profile analysis indicates a full width half maximum (FWHM) of 0.64 μm, which is comparable to the theoretical axial profile FWHM of ∼0.55 μm calculated by the following equation:[17]

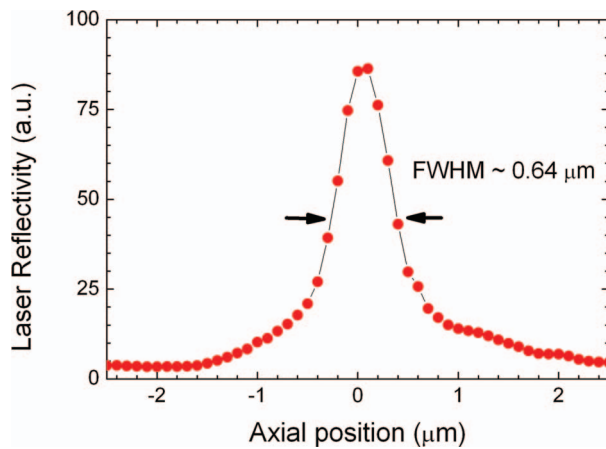$$FWHM = \frac{Q \cdot \lambda}{n - \sqrt{n^2 - NA^2}}. \tag{1}$$

FIG. 3. Axial profile of the laser reflection from a Si sample reveals the axial resolution of our confocal micro-Raman system to be ∼0.64 μm.
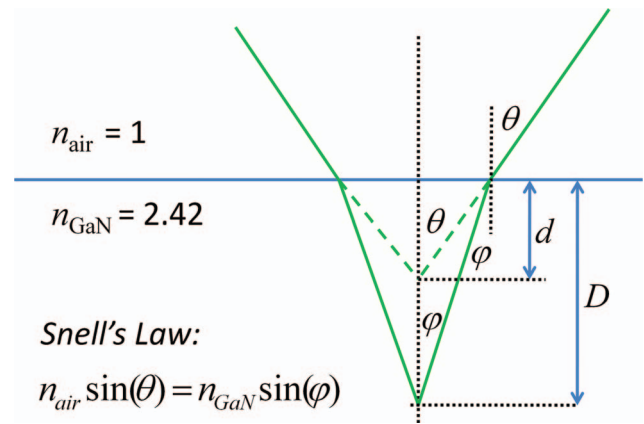

FIG. 4. Ray tracing based on Snell's law illustrates that the refraction index mismatch shifts the focusing position, where d and D denote the depth of the intended and actual focus spot, respectively, for a ray incident at an angle θ.

In Eq. (1), λ is the excitation wavelength, and n is the refraction index of the immersion medium. The value of the factor Q depends on the type of sample, the excitation wavelength, detection pinhole size, and the combined objective and tube lens magnification. There is no analytical expression for Q, and the details of the dependence including numerically calculated results can be found in Ref. 17. For our system of 100×, 0.9NA objective and core diameter 50 μm optical fiber, it equals to having a 0.69 Airy unit (AU) size pinhole, where 1 AU = 1.22λ/NA. This pinhole size corresponds to a Q value of 0.58 when confocal measurement is performed on a reflecting surface sample. Substituting this Q value into Eq. (1) leads to an axial profile with FWHM ∼0.55 μm. For layered epitaxial samples such as the LED sample studied in this study, the Q value increases by a factor of 1.56 in comparison to a reflecting surface sample.[17] Therefore, the axial resolution of our system is estimated to be ∼1 μm at sample surface when one performs depth-resolved micro-Raman spectroscopy measurements on GaN-based LED structures.

B. Focal point shift and axial resolution degradation due to the refraction index mismatch

Depth calibration is a crucial task when one intends to resolve the embedded LED layer structure with confocal optical microscope. Due to the refraction index difference between the sample and the immersion medium of the objective, the actual focus position inside the sample is deeper than the physical movement of the Z-piezo stage. A simple ray tracing diagram clearly illustrates this depth compression effect in Figure 4. As the light ray intended for focus depth d enters the sample at angle θ, it is refracted at the sample surface due to Snell's law and is in fact focused at a greater depth D. As a result of the focal shift to a greater depth, axial scan measurement by stage translation over a smaller distance d leads to a larger actual scanned depth D inside the sample. It is worth to note that an axial plot of the acquired experimental data from 0 to d in fact reflects the measurement of an actual depth from 0 to D, which results in a *compression* of the actual axial profile. The amount of focal shift D-d depends not only on the intended focus depth d, but also on the angle of

incidence θ. The excitation light entering the objective consists of rays with angle θ from 0 to a maximum angle θ_{max} determined by the objective numerical aperture, NA = $\sin(\theta_{max})$. Using geometric optics analysis and averaging over $\theta = 0$ to $\theta = \theta_{max}$, Baldwin and Batchelder have derived an equation to determine the mean focal depth.[18] With their equation and a refraction index of 2.42 for GaN at 532 nm,[19] we obtain a theoretical depth compression factor D/d, of 3.7. To correctly indicate the axial focal position inside the LED sample, we rescale the axial position of the piezo stage from the sample surface by this compression factor to reflect the real focal position. It is worth to point out that in addition to changing the focal depth, the refraction index mismatch also degrades the axial size of the focal point which we use as the indicator of the axial resolution. Baldwin and Batchelder have also derived an equation for the axial size of the focal point defined as the range where 50% of light intensity is contained.[18] Following their derivation, we approximates the axial illumination profile by a Gaussian distribution function, where the 50% light intensity point (area under the distribution curve) occurs at ±0.67σ, and σ is the standard deviation for the Gaussian function. Using the equation derived by Baldwin and Batchelder[18] we obtain for the objective in use, an axial size of the focal point equal to 0.26 D, where D is the actual focal depth inside GaN.[15] The shift of the laser focal spot with depth means that the axial resolution also becomes worse with increasing depth.[18,20] It implies the obtained ∼1 μm axial resolution described in Sec. III A can only hold at the sample surface.

C. Depth-dependent Raman spectra

Figure 5 shows the spectra of the GaN LED sample at various depths, where the origin is set at sample surface and increases towards the sample. The depth of focus inside the sample has been determined by multiplying the position change of the objective piezo stage by the theoretically calculated depth compression factor of 3.7 as described in Sec. III B. The four spectra are acquired at depths of −0.5 μm, 0.9 μm, 3.7 μm, and 14.8 μm corresponding to (A) near the sample surface, (B) the location of
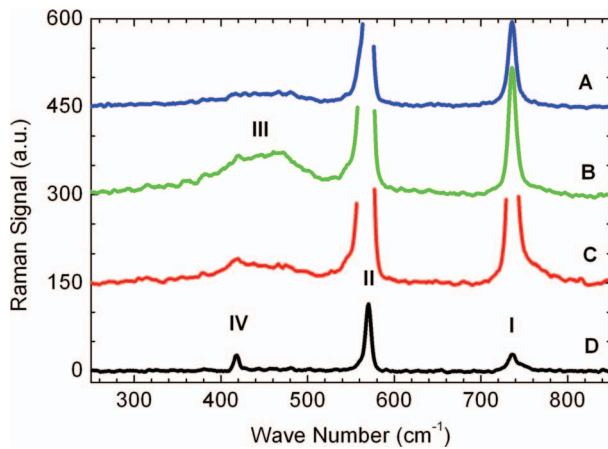
FIG. 5. Raman Spectra at different depths of the sample from the sample surface (0 μm) toward the sapphire substrate. The corresponding depths of the four Raman spectra are: (A) near sample surface at -0.5 μm, (B) MQW active layer at 0.9 μm, (C) n-GaN at 3.7 μm, and (D) inside the sapphire substrate at 14.8 μm. The Roman numeral labels indicate the corresponding phonon peaks: (I) GaN A_1(LO) at 736 cm^{-1}, (II) GaN E_2(high) at 570 cm^{-1}, (III) a broad double peak feature originated from the MQW active layer, and (IV) sapphire A_{1g} at 417 cm^{-1}. Note that due to the large intensities of GaN A_1(LO) and E_2(high) peaks, all the spectra have been truncated to fit into the displayed area.
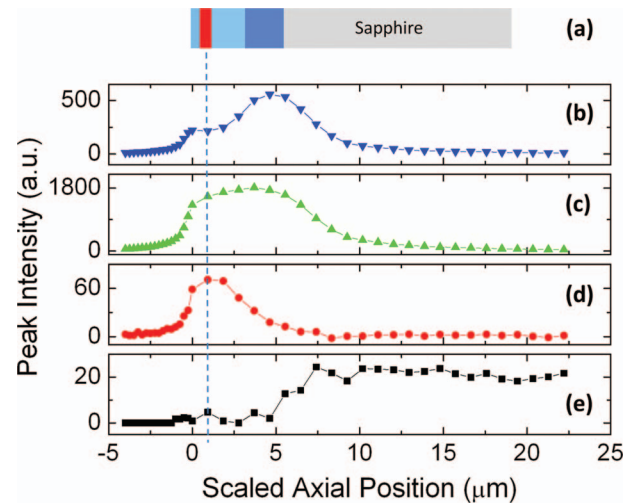

FIG. 6. Axial profile of the phonon peaks marked in Figure 5. (a) Diagram of the sample layer structure, where the layers from left to right are the p-GaN capping layer, MQW/superlattice active layer, n-GaN, u-GaN, and sapphire substrate, respectively. The axial profiles shown are: (b) GaN A_1(LO) phonon, (c) GaN E_2(high) phonon, (d) MQW active layer phonon feature, and (e) sapphire A_{1g} phonon, respectively.

MQWs/superlattice, (C) the n-GaN and u-GaN region, and (D) the sapphire substrate region, respectively. A constant offset of 150 is added to each sequential spectrum to facilitate their display. Due to the huge Raman contributions of GaN A_1(LO) at 736 cm^{-1} and E_2(high) at 570 cm^{-1}, their spectral features are even observable in the near sample surface region. In the location of MQWs/superlattice layer, the Raman spectrum clearly reveals a broad feature peak in the range of 419–465 cm^{-1}, which is associated with the interfacial phonon of the MQWs/superlattice. This observation successfully demonstrates the capability of our optical system even though the 0.2 μm thin MQWs/superlattice region is much less than the system axial resolution. The spectrum at depth 3.7 μm located inside the n-GaN and u-GaN region shows the strongest intensities for the two GaN lines. At 14.8 μm depth, the spectrum reveals the sapphire A_{1g} phonon at 417 cm^{-1} in addition to a relatively weak signal from the GaN layer.

D. Identification of phonon structure in the LED active layer

In Figure 6 the axial profiles of the peak features (I–IV) shown in Figure 5, are plotted to clearly illustrate the phonon contributions from different layers of the LED sample. Each axial profile is constructed by analyzing the peak position and intensity of all depth-dependent Raman spectra acquired by varying the Z-piezo stage position in steps of 0.25 μm. Figure 6(a) is the LED sample diagram showing the relative position of the various layers for reference. A dashed line is drawn to indicate the position of the MQWs/superlattice. In Figure 6(b), the two peak features of GaN A_1(LO) axial profile correspond to the two GaN regions above and below the MQWs/superlattice. In Figure 6(c), GaN E_2(high) axial profile is similar to that of GaN A_1(LO), except the dip is not as

prominent in the MQWs/superlattice region. The axial profile of the 465 cm^{-1} shown in Figure 6(d) consistent with MQWs/superlattice layer located between the p-GaN and n-GaN regions. In Figure 6(e), sapphire A_{1g} axial profile remains fairly constant from inside the substrate and falls to approximately half of that constant value at $\sim$6 μm. The position of the drop coincides with the position where the intensity of the GaN A_1(LO) and E_2(high) axial profile rises to its peak. The axial profiles for each phonon peaks consistent with the LED sample structure illustrated in Figure 1.

As described in Sec. III B, it is expected that the refraction index mismatch not only results in depth compression, but also degrades the point spread function.[18,20] At the GaN/sapphire interface (at depth of 6 μm), the axial size of the focal point described as the distance containing 50% of integrated light intensity, has a theoretical value of 0.26*6 μm = 1.6 μm (Sec. III B). Experimentally, this axial size of the focal point corresponds to the distance over which the GaN axial profiles in Figure 6 falls at the GaN/sapphire interface from 75% to 25% of the maximum. For the GaN A_1(LO), GaN E_2(high) profile shown in Figures 6(a) and 6(b), the axial size of the focal point at 6 μm corresponds to 2.2 μm and 2.6 μm, respectively. Similarly for the sapphire A_{1g} axial profile, the rise from 25% to 75% of the maximum value occurs over a distance of 1.9 μm. The axial sizes of the focal point derived from the axial profiles are consistent with the theoretical predictions to within 1 μm, which corresponds to the step-size used for the acquired axial data. The variation can be attributed to the axial resolution degradation with increasing focal depth (Sec. III B), thus causing the peak profile to fall more slowly with depth.

E. Strain distribution from the sapphire substrate toward the LED surface

Due to the lattice mismatch between GaN and the sapphire substrate, the local strain near the GaN/sapphire
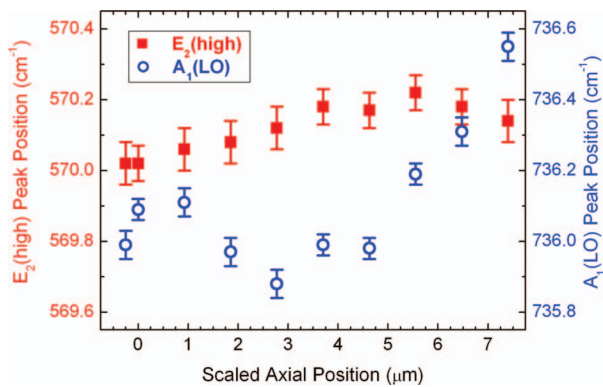
FIG. 7. The peak frequencies of the GaN A_1(LO) and E_2(high) phonon modes are plotted as a function of the sample depth from the sample surface toward the sapphire substrate. The peak positions and error bars are determined by least-square curve fitting the Raman peak with single Gaussian function.

interface is often predicted and expected. In this work, we also try to realize the possible strain distribution as a function of the sample depth with our technique. By curve-fitting the GaN A_1(LO) and E_2(high) Raman peak profiles of the depth-dependent Raman spectra, we are able to determine the Raman peak position to a precision of $\sim$0.1 cm^{-1}. Figure 7 plots the peak position of GaN A_1(LO) and E_2(high) phonons as a function of the sample depth, from the sample surface toward the GaN/sapphire interface. The error bars reflect the uncertainty in the curve-fitting. Since the phonon frequency shift is linearly proportional to both the biaxial and uniaxial strain in GaN,[21,22] the obtained depth profiles in Figure 7 reveals the strain distribution from the sapphire substrate to the LED surface. Since A_1(LO) and E_2(high) phonon frequencies occur at 734 cm^{-1} and 568 cm^{-1} for unstrained GaN bulk, respectively,[9] we argue that the trend of frequency shift in both phonon modes indicate the relaxation of compressive strain from the GaN/sapphire interface toward the LED surface. Theoretical calculations shows that the shift in A_1(LO) is more sensitive to the uniaxial strain along the c-axis, while the shift in E_2(high) is more sensitive to the biaxial strain along the c-plane of GaN.[22] Therefore, the larger frequency shift in A_1(LO) compared to E_2(high) reveals that from the sapphire substrate to the sample surface, there is a greater change in the uniaxial strain along the growth direction than the biaxial strain in the sample plane. Furthermore, Figure 7 implies that significant strain remains in the active area near the surface of the LED structure, because even at the sample surface, the measured frequencies of both A_1(LO) and E_2(high) phonons are still larger than those of unstrained GaN bulk reported in literature.[9]

IV. CONCLUSIONS

We have demonstrated the layer structure of GaN-based LED can be successfully determined with depth-resolved confocal micro-Raman spectroscopy. The refraction index mismatch between GaN and air for the NA0.9 objective

results in a significant depth compression factor of 3.7. When the depth compression correction is properly taken into account, the axial Raman peak intensity profiles can correctly correspond to the designed sample structure. The scaled axial profiles of the Raman peak intensities allow us to identify a unique MQWs/superlattice Raman feature originated from the thin LED active layer. The frequency shifts of GaN A_1(LO) and E_2(high) phonon modes along the axial direction provide quantitative description of the GaN strain distribution at different layers inside the sample. The ability to characterize the active layer and the strain axial change makes this depth-resolved confocal micro-Raman spectroscopy a potential powerful technique to *in operando* explore many important electronic and structural problems associated with GaN-based optoelectronic devices.

[1] J. S. Speck and S. F. Chichibu, MRS Bull. **34**, 304 (2009).
[2] F. Scholz, Semicond. Sci. Tech. **27**, 024002 (2012).
[3] J. Piprek, Phys. Status Solidi A. **207**, 2217 (2010).
[4] K. J. Vampola, M. Iza, S. Keller, S. P. DenBaars, and S. Nakamura, Appl. Phys. Lett. **94**, 061116 (2009).
[5] Y. C. Shen, G. O. Mueller, S. Watanabe, N. F. Gardner, A. Munkholm, and M. R. Krames, Appl. Phys. Lett. **91**, 141101 (2007).
[6] T. Wilson, *Confocal Microscopy* (Academic Press, London, 1990).
[7] J. B. Pawley, *Handbook of Biological Confocal Microscopy* (Kluwer Academic Publishers, 1995).
[8] V. P. Kladko, A. F. Kolomys, M. V. Slobodian, V. V. Strelchuk, V. G. Raycheva, A. E. Belyaev, S. S. Bukalov, H. Hardtdegen, V. A. Sydoruk, N. Klein, and S. A. Vitusevich, J. Appl. Phys. **105**, 063515 (2009).
[9] H. Harima, J. Phys.: Condens. Matter **14**, R967 (2002).
[10] H. Siegle, P. Thurian, L. Eckey, A. Hoffmann, C. Thomsen, B. K. Meyer, H. Amano, I. Akasaki, T. Detchprohm, and K. Hiramatsu, Appl. Phys. Lett. **68**, 1265 (1996).
[11] V. V. Strelchuk, V. P. Kladko, E. A. Avramenko, O. F. Kolomys, N. V. Safryuk, R. V. Konakova, B. S. Yavich, M. Y. Valakh, V. F. Machulin, and A. E. Belyaev, Semiconductors **44**, 1199 (2010).
[12] M. J. Matthews, A. L. Harris, A. J. Bruce, and M. J. Cardillo, Rev. Sci. Instrum. **71**, 2117 (2000).
[13] N. J. Everall, Appl. Spectrosc. **54**, 773 (2000).
[14] C. H. Wang, S. P. Chang, W. T. Chang, J. C. Li, Y. S. Lu, Z. Y. Li, H. C. Yang, H. C. Kuo, T. C. Lu, and S. C. Wang, Appl. Phys. Lett. **97**, 181101 (2010).
[15] Y. L. Li, T. Gessmann, E. F. Schubert, and J. K. Sheu, J. Appl. Phys. **94**, 2167 (2003).
[16] R. Charash, P. P. Maaskant, L. Lewis, C. McAleese, M. J. Kappers, C. J. Humphreys, and B. Corbett, Appl. Phys. Lett. **95**, 151103 (2009).
[17] S. Wilhelm, B. Grobler, M. Gluch, and H. Heinz, *Confocal Laser Scanning Microscopy: Principles* (Zeiss Jenna, 2003).
[18] K. J. Baldwin and D. N. Batchelder, Appl. Spectrosc. **55**, 517 (2001).
[19] M. Bass, V. N. Mahajan, E. W. Van Stryland, G. Li, C. A. MacDonald, C. DeCusatis, and Optical Society of America, *Handbook of Optics*, 3rd ed. (McGraw-Hill, New York, 2010).
[20] N. J. Everall, Appl. Spectrosc. **63**, 245A (2009).
[21] F. Demangeot, J. Frandon, M. A. Renucci, O. Briot, B. Gil, and R. L. Aulombard, Solid State Commun. **100**, 207 (1996).
[22] J. M. Wagner and F. Bechstedt, Appl. Phys. Lett. **77**, 346 (2000).